

Influence of refractive-index mismatch in high-resolution three-dimensional confocal microscopy

Alberto Diaspro, Federico Federici, and Mauro Robello

The effects of the refractive-index mismatch in confocal laser scanning microscopy were extensively studied. The axial aberration induced in the case of fluorescent microspheres was measured. The data were used to take into account the mismatch-induced aberrations and to consider object-size influence. Then we focused on the effect of refractive-index mismatch on the effective system's point-spread function under different mismatch conditions and on depth of focusing. We experimentally verified that the peak of the point-spread function intensity profile decreases and the point-spread function itself progressively broadens as a function of the combined effect of the refractive-index mismatch and of the penetration depth, leading to a worsening of the system's overall performances. We also performed these same measurements by embedding subresolution beads in an oocyte's cytoplasm, which can be considered a turbid medium. We found evidence consistent with the previously developed theoretical model; in particular we found a strong dependence of the intensity peak on the focusing depth. © 2002 Optical Society of America

OCIS codes: 180.1790, 180.6900, 180.2520, 080.2710, 080.1010, 170.3880.

1. Introduction

Far-field light microscopy, encompassing conventional and confocal fluorescence, is the most widely applied form of microscopy in biological research.¹⁻³

The confocal microscope, especially in its confocal laser scanning configuration, couples three-dimensional properties with high-resolution imaging.⁴⁻⁷ In fact, it allows us to discriminate details with a lateral resolution that is 1.4 times better than that of the conventional microscope and it has the ability to resolve objects in the third (axial) direction.⁸ In confocal laser scanning microscopy (CLSM) only in-focus light is imaged through an optical-ray-selective aperture, i.e., a pinhole, whereas out-of-focus rays are physically rejected by the opaque parts of the pinhole. This results in an optical sectioning ability that is absent in conventional optical microscopy.⁹⁻¹² CLSM thus provides efficient and noninvasive optical sections through thick biological

samples while preserving, at the same time, their three-dimensional structure. Unfortunately, one of the major limitations to its practical application is that the imaging performance can be altered when we are focusing into a medium whose refractive-index amplitude and phase components do not match those transversed by the light before reaching the sample; we refer to this condition as refractive-index mismatch.¹³⁻¹⁹ So far, geometric distortions and deterioration of the point-spread function (PSF) that are due to refractive-index mismatch between the medium containing the biological object under investigation and the medium where light propagates are of particular interest and also play a role in the field of image restoration.²⁰⁻²²

In this paper we deal with some of the effects that are due to the refractive-index mismatch in the case of CLSM performed under a fluorescence regime and with a high numerical-aperture (NA) objective.

As the first step, we measured the axial aberration induced by such a mismatch in the case of fluorescent objects of well-known spatial extension, i.e., microspheres of known diameter. We analyzed the data, reporting the way they can be used to take into account the mismatch-induced aberrations and to consider object-size consequences. This is particularly relevant in those studies dealing with morphometrical analysis of samples and with the spatial localization of fluorescently labeled structures in the sample space. The results of this first step have been used

The authors are with the Istituto Nazionale per la Fisica della Materia, National Institute for the Physics of Matter, and the Department of Physics, University of Genoa, Via Dodecaneso 33, 16146 Genoa, Italy. A. Diaspro's e-mail address is diaspro@fisica.unige.it.

Received 13 April 2001; revised manuscript received 6 August 2001.

0003-6935/02/040685-06\$15.00/0

© 2002 Optical Society of America

to correctly perform the analysis related to the successive steps.

As the second step, we focused on the influence of refraction-index mismatch on the characteristics of the PSF of the microscope under different mismatch conditions and with different depths of focusing.

In this case, we used subresolution fluorescent beads and a geometry that allows us to take into account the different depth-of-focus conditions in different media. This has led to some important insights about system resolution in terms of the effective PSF. According to previously developed theoretical approaches,^{15,16,23} we experimentally verified that the peak of the PSF intensity profile decreases and the PSF itself progressively broadens (especially along the optical axis direction) as a function of the combined effect of the refractive-index mismatch and of the penetration depth, leading to a worsening of the system's overall performances.

As the third step, we repeated the same measurements of the second step by embedding subresolution beads in a medium whose absorption and scattering properties are no longer negligible and thus can be considered turbid. We found evidence of the phenomena so far discussed (broadening of the PSF and weakening of the emission signal); in particular we found a strong exponential dependence of the intensity peak on the focusing depth. It is, however, hard to give a true quantitative meaning to these last measurements, as the strong inhomogeneity inside the medium causes our results to be just an approximate description of the real capabilities of the system and as there is no precise theory about focusing a laser beam inside a turbid medium because of the difficulties in mathematically modeling such a situation. Computer simulations have been developed,¹⁸ including the introduction of an effective PSF, but experimental analysis is still the most widespread approach.

2. Materials and Methods

A. Confocal Laser Scanning Microscopy Imaging

We used a compact CLSM system (PCM2000, Nikon Spa, Florence, Italy) based on a galvanometer point-scanning mechanism, a single-pinhole optical path, and an efficient all-fiber optical system for light delivery, in both excitation and in collection. We used a Nikon 60× air-immersion objective (NA = 0.85; WD = 0.30 mm, where WD is the working distance) and a Nikon 100× oil-immersion objective ($n = 1.52$; NA = 1.30; WD = 0.20 mm). The whole system has been described in detail elsewhere.²⁴ The all-fiber solution avoids a dangerous vibration decoupling between the laser source and the scanning head even if they are placed on different tables. Moreover, by use of three mechanically fixed possible pinhole diameters (20 μm , 50 μm , and open), it is possible to repeat the same effect with excellent reproducibility and system stability. The 20- μm -diameter pinhole resulted in a backprojected radius two times smaller than that of the backprojected Airy disk when the

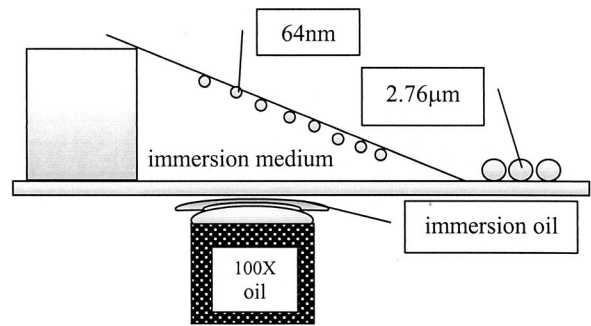


Fig. 1. Experimental setup for evaluating the focusing depth of the subresolution beads. The PSF's depth in the mounting medium was evaluated by defocusing with respect to a sample of 2.76- μm -diameter microspheres. This value was then been corrected by use of the experimental scaling factor to account for the refractive-index mismatch.

100× objective was used. The scanning head was mounted on an inverted optical microscope Nikon Eclipse TE 300. Images were collected with the 488-nm laser line for excitation and a 515/30-nm-emission optical filter. R928 photomultiplier tubes (Hamamatsu, Shizuoka, Japan) were used.

B. Microspheres for Axial Aberration Measurements

Different sets of reference objects, i.e., microspheres, were used, namely, latex microspheres loaded with yellow-green fluorescent dye (Polysciences, Warrington, Pa.), whose diameters were (2.76 ± 0.06) , (15.24 ± 1.22) , and (21.99 ± 2.69) μm . A drop of a water-diluted sample was put on a glass coverslip of 0.17-mm nominal thickness and air dried in a dust-free chamber.

A drop of a different medium, i.e., glycerol, $n = 1.48$, immersion oil, $n = 1.52$, or liquid NOA 61 (Norland, New Brunswick, N.J.), $n = 1.53$, was deposited on the dried sample in order to test different refractive-index mismatch conditions.

C. Point-Spread Function Measurements as Functions of Refractive-Index Mismatch and Penetration Depth

An optical section of latex subresolution beads ($\varnothing = 64$ nm) loaded with yellow-green fluorescent dye (Polysciences, Warrington, Pa.) was recorded with a 20- μm pinhole aperture size and a 100× oil-immersion objective. Beads were sampled at 100-nm steps along the z axis and at 28 nm in the xy plane. They were located deep in the immersion medium, with the geometry depicted in Fig. 1. To minimize photobleaching, a neutral-density filter was also used along the excitation pathway.

PSFs were collected for three different immersion media: air, oil ($n = 1.52$), and glycerol ($n = 1.48$). No absorption in the range of the considered wavelengths was found from spectrophotometric measurements (data not shown).

The depth of each recorded PSF was estimated by defocusing with respect to the bottom of a set of 2.76- μm -diameter microspheres dried beside the sample (Fig. 1). This procedure was repeated several times

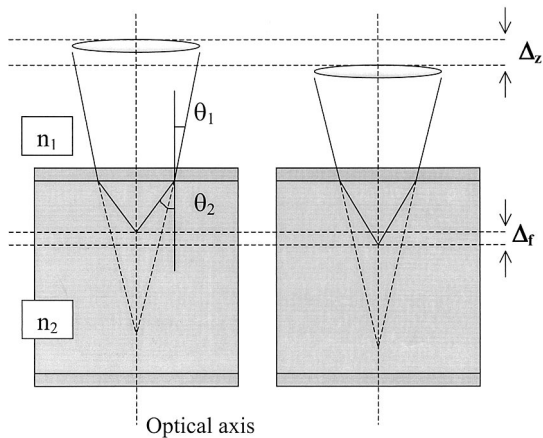


Fig. 2. Experimental conditions typically encountered when one is focusing inside a medium whose refractive index does not match that of the objective. A convergent light wave traveling through a medium with refractive index n_1 (objective-immersion medium) is focused by the objective into a second medium (sample-immersion medium with refractive index n_2). The marginal rays make an angle θ_1 with the normal to the interface and an angle θ_2 after refraction. In this plot we consider the case $n_1 > n_2$.

to evaluate positioning error (<5%). Moreover, to somehow take into account the presence of a refractive-index mismatch, the evaluated distances were then scaled down by use of the measured experimental scaling factors, referring to 2.76- μm -diameter microspheres.

D. Point-Spread-Function Measurements in Turbid Media as Functions of Depth

Images of subresolution beads (64-nm diameter) were recorded in a *Xenopus Laevis* oocyte's cytoplasm that acted as absorbing and scattering medium (spectrophotometric data not shown) because of its content of proteins and RNA needed for cell division and growth. We chose this sample medium because of the large amount of material available and the popularity of *X. Laevis* oocytes in the study of many developmental mechanism and basic cellular processes.

The same experimental setup as that described in the preceding subsection was used to evaluate the sample's focusing depth.

3. Results

A. Axial Aberration

The situation that we typically encounter when focusing in the presence of a refractive-index mismatch is shown in Fig. 2.

Under the assumption of neglecting the coverslip refractive index, a rigorous treatment with geometric optics^{14,17} leads to the following analytical relationship between the distance Δ_z scanned by the objective along the optical axis and the corresponding distance

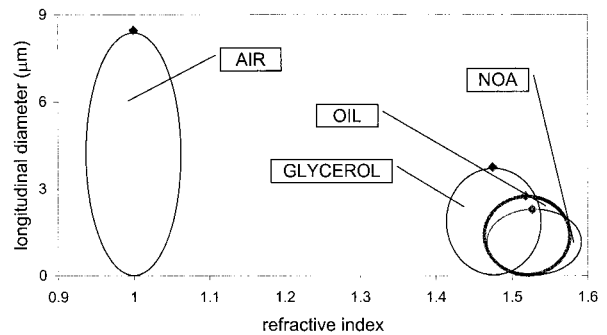


Fig. 3. Side view (xz plane) of the 2.76- μm fluorescent microspheres embedded in different media with known refractive indices. The spheres immersed in oil appear to be “more” spherical than the others.

Δ_f actually scanned by the focused spot within the sample space:

$$\Delta_f = \frac{n_2}{n_1} \left[\frac{1 - \left(\frac{n_1}{n_2} \sin \theta_1 \right)^2}{\cos \theta_1} \right]^{1/2} \Delta_z. \quad (1)$$

By using of Eq. (1), we can immediately foresee that whenever $n_1 > n_2$ (respectively, $n_1 < n_2$) the axial elongation of the object measured by the system is greater (less) than the real one. A three-dimensional image of each microsphere was recorded as a set of optical slices at 200-nm steps. The measure was repeated for the different pinhole aperture sizes.

The results of the axial elongation with respect to the real size of the object are shown in Fig. 3, where we have plotted the averaged values of z diameters versus the refractive index of the immersion medium for the case of 2.76- μm -diameter microspheres, 100 \times oil-immersion objective, and 20- μm pinhole aperture size. As can be immediately seen, the least axial aberration is found in the case of oil-immersed microspheres, which is the minimized mismatch one. This is consistent with the previously developed theory, which, however, is apparently a good tool for describing the trend of axial elongation from only a qualitative point of view.

On the other hand, Eq. (1) cannot be taken into account for directly calculating a scaling factor Δ_z/Δ_f to resize any distance along the optical axis: As far as we know, it does not adequately fit experimental values. This is because of, among other things, its strong dependence on θ_1 .

A more a precise relationship could be found by consideration of some average over the imaged object shape: This, however, would be of no great help in practice, because it requires an *a priori* knowledge of the sample properties and may require quite a lot of time for calculations. We can now figure out how the scaling factor depends on the object size.

The scaling Δ_z/Δ_f keeps nearly constant within a 50% object size variation (Fig. 4). This leads us to conclude that whenever we need to account for axial

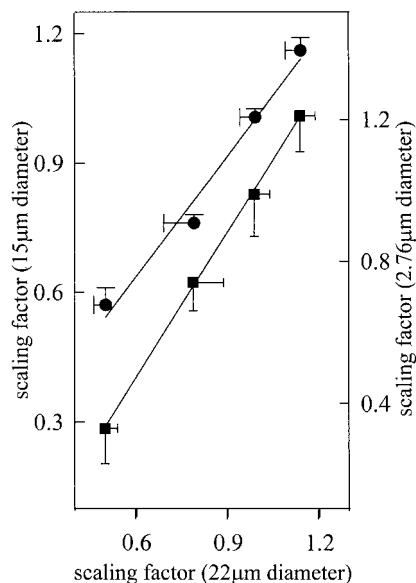


Fig. 4. Graph of the average scaling factor for different mismatch conditions for 22- μm -diameter versus 3- μm -diameter microspheres (square) and versus 15- μm diameter microspheres (circles). Each point on the graph is the average over 20 microspheres. The data were fitted according to a linear relationship, $y = ax + b$, in order to point out the dependence of the scaling factor on the object size. The best-fit parameters are $a = 1.36$ and $b = 0.35$ with a 99% correlation (for squares) and $a = 0.94$ and $b = -0.07$ with a 98% correlation (for circles).

aberration, we can recover an effective scaling factor by embedding microspheres whose diameter is comparable with that of the sample size in the sample medium.

B. Effects of Refractive-Index Mismatch on the Point-Spread Function as a Function of Penetration Depth

Table 1 reports the evaluation of the lateral and the axial resolutions (FWHMs) as functions of the focusing depth and the immersion medium's refractive index.

As shown in Fig. 5, the PSF tends to be more and more broadened as the focusing depth increases, in agreement with earlier theoretical data.¹⁵ This phenomenon is more evident along the optical axis: This is the reason the system axial resolution gets worse and worse rather than that of the lateral resolution. The trend reported in figures and tables

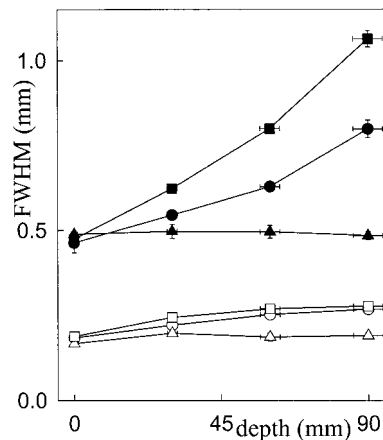


Fig. 5. Plot of the lateral FWHM (open circles) and axial FWHM (filled circles) versus focusing depth for the oil-immersed PSF (triangles), glycerol-immersed PSF (circles), and air-immersed PSF (squares). Each point given on the graph is the average over 30–40 PSFs at the corresponding focusing depth.

becomes even more noticeable under refractive-index mismatch conditions.²⁵

As a consequence of this fact, the largest percentage of variation of the lateral FWHM, with respect to the focusing depth, swings from 6% (oil-immersed PSF) to 48% (air-immersed PSF) whereas the axial FWHM varies up to 130% (air-immersed PSF).

In Table 2 the percentage of variation (with respect to the 0- μm depth of focus) of the PSF intensity peak in different mismatch conditions is reported as a function of the focusing depth.

This points out the weakening of the signal with respect to the focusing depth: This phenomenon turns out to be more evident in the case of air-immersed samples, when the maximum refractive-index mismatch is present.

We can neglect any remarkable absorption phenomenon as a consequence of the spectrophotometric analysis on the media (data not shown).

C. Point-Spread Function Measurements in Turbid Media as Functions of Penetration Depth

The analysis of the experimental results referring to the broadening of the PSF (thus to the worsening of the axial and the lateral resolutions) has given results similar to the preceding ones, although, because of the strong inhomogeneities inside such a medium,

Table 1. Lateral and Axial FWHMs as Functions of the Focusing Depth and the Immersion Medium's Refractive Index^a

Depth (μm)	Air		Glycerol		Oil	
	Lateral (nm)	Axial (nm)	Lateral (nm)	Axial (nm)	Lateral (nm)	Axial (nm)
0	187 \pm 8	484 \pm 24	183 \pm 14	495 \pm 29	186 \pm 6	489 \pm 6
30	244 \pm 10	623 \pm 9	221 \pm 5	545 \pm 12	197 \pm 10	497 \pm 21
60	269 \pm 11	798 \pm 10	252 \pm 7	628 \pm 9	186 \pm 12	496 \pm 19
90	277 \pm 5	1063 \pm 24	268 \pm 8	797 \pm 26	191 \pm 9	484 \pm 12

^aLateral and axial FWHMs for PSF immersed in different media at different focusing depths. Standard error refers to an average over a set of 30–40 PSF. The objective used is a 100 \times oil-immersed one.

Table 2. Percentage of Variation of the PSF Intensity Peak in Different Mismatch Conditions as a Function of the Focusing Depth^a

Medium	% at 30 μm	% at 60 μm	% at 90 μm
Oil	3	6	7
Glycerol	17	27	34
Air	44	51	60
Cytoplasm	65	88	96 ^b

^aPercentage of variation of the PSF intensity peak with respect to the 0- μm focusing-depth intensity peak for the different media. The objective used is a 100 \times oil-immersed one.

^bExtrapolated from the experimental trend.

we can only semiquantitatively rely on them. In the last row of Table 2 we report the percentage of variation (with respect to the 0- μm depth of focus) of the PSF intensity peak in cytoplasm. To account for the strong decrease of the intensity peak on the focusing depth, we introduce an effective objective aperture angle.

Under the assumption that the light intensity effectively recovered by the objective is proportional to the area of the objective hit by the fluorescence emission radiation, we may come to the following relationship:

$$\frac{I_0 - I_1}{I_0} = \frac{tg^2\alpha_0 - tg^2\alpha_1}{tg^2\alpha_0}, \quad (2)$$

where α_0 and α_1 are the effective maximum aperture angles of the objective, referring to two different refractive-index mismatch and depth-of-focus conditions, and I_0 and I_1 are the corresponding light intensity.

By substituting into I_0 the value of the PSF intensity at 0- μm focusing depth in oil (for which $\alpha_0 = 60^\circ$) and into I_1 the value referring to the PSF at 0 μm in the cytoplasm, we may get $\alpha_1 = 52^\circ$.

The difference between these two angles, leading to a growing decrease in the collected light with respect to the depth of focus in mismatch conditions, might somehow couple with the preceding theories and account for the strong weakening of the PSF intensity peak, which is due to the particular scattering property of the medium. The decreasing peak intensity value of the PSF at 90 μm could thus be explained if we consider that the effective maximum objective angle is $\alpha_1 = 14^\circ$, whereas $\alpha_0 = 60^\circ$ in the perfectly matched situation of a nonscattering, nonabsorbing medium.

4. Conclusions

In this paper we have discussed the effect of a refractive-index mismatch over a confocal system's performances both in terms of a morphometrical analysis of specimens and of a PSF, which allowed us to obtain information about resolution and the penetration limit.

The experimental method suggested for scaling the distance along the optical axis is needed when we are trying to precisely locate objects within any sample whose refractive index does not perfectly match that

of the objective-immersion medium: We have found that the scaling factor, which accounts for the refractive-index mismatch, stays nearly constant within a 50% object-size variation. This leads us to conclude that whenever we need to account for axial aberration, we can recover an effective scaling factor by embedding microspheres whose diameter is comparable with the sample size in the sample medium.

On the other hand, the study of the experimental PSFs has given results consistent with the theory recovered in literature: The PSF tends to be more and more broadened and asymmetric as the focusing depth increases. This phenomenon is even more evident along the optical axis: This is the reason the system axial resolution gets worse and worse rather than the lateral resolution. The trend becomes even more effective under refractive-index mismatch conditions. Moreover, the PSF's intensity peak gets smaller and smaller under growing mismatch conditions: This points out a weakening of the signal with respect to the focusing depth.

This has allowed us to learn the actual system resolution in the mismatch situation considered and to verify to what extent it depends on the focusing depth. The experimental PSFs collected can be eventually used to implement deconvolution algorithms.

In the course of these different studies, we have also taken into account the particular case of a turbid medium. It has been possible to get some insight about its absorption and scattering properties directly from the analysis of the collected PSFs. However, the lack of a reliable and practicable theory and the intimate inhomogeneity of the medium still prevent us from considering our numerical results as quantitatively meaningful.

To account for the strong decrease of the intensity peak on the focusing depth in this turbid medium, we introduced an effective objective aperture angle: This has shown that a decrease in the intensity peak goes with a decrease in the effective objective angle, which is due to the high scattering property of the medium itself. We have found that the reduced image quality when refractive-index mismatch occurs is of great importance for the imaging quality, especially during deep measurement into samples: The progressive broadening of the system impulse response and its decreasing intensity peak accounts for this phenomenon. This turns out to be even more evident when we are dealing with thick biological turbid media, such as oocyte's cytoplasm, as the absorption and scattering properties are no longer negligible and cause the PSF to be nonspace invariant, strongly asymmetric, and broadened, thus worsening spatial resolution.

References

1. D. M. Shotton, "Confocal scanning optical microscopy and its applications for biological specimens," *J. Cell. Sci.* **94**, 175–206 (1989).
2. A. Diaspro, ed. *Confocal and Two-Photon Microscopy: Found-*

- dations, Applications, and Advances* (Wiley-Liss, New York, 2001).
3. R. H. Webb, "Confocal optical microscopy," *Rep. Prog. Phys.* **59**, 427–471 (1996).
 4. M. Minsky, "Microscopy apparatus," U.S. patent 3,013,467 (19 December 1961).
 5. C. J. R. Sheppard and A. Choudhury, "Image formation in the scanning microscope," *Opt. Acta* **24**, 1051–1073 (1977).
 6. T. Wilson and C. J. R. Sheppard, *Theory and Practice in Scanning Optical Microscopy* (Academic, London, 1984).
 7. J. G. White, W. B. Amos, and M. Fordham, "An evaluation of confocal versus conventional imaging of biological structures by fluorescence light microscopy," *J. Cell Biol.* **105**, 41–48 (1987).
 8. G. J. Brakenhoff, P. Blom, and P. Barends, "Confocal scanning light microscopy with high aperture immersion lenses," *J. Microsc.* **117**, 219–232 (1979).
 9. B. Bianco and A. Diaspro, "Analysis of the three dimensional cell imaging obtained with optical microscopy techniques based on defocusing," *Cell Biophys.* **15**, 189–200 (1989).
 10. C. J. R. Sheppard, "Axial resolution of confocal fluorescence microscopy," *J. Microsc.* **154**, 237–242 (1989).
 11. T. Wilson, "Optical sectioning in confocal fluorescent microscopes," *J. Microsc.* **154**, 143–156 (1989).
 12. A. Diaspro, M. Sartore, and C. Nicolini, "Three-dimensional representation of biostructures imaged with an optical microscope. I. Digital optical sectioning." *Image Vision Comput.* **8**, 130–134 (1990).
 13. K. Carlsson, "The influence of specimen refractive index, detector signal integration, and non-uniform scan speed on the imaging properties in confocal microscopy," *J. Microsc.* **163**, 167–178 (1991).
 14. T. D. Visser, J. L. Oud, and G. J. Brakenhoff, "Refractive index and axial distance measurements in 3-D microscopy," *Optik* **90**, 17–19 (1992).
 15. S. Hell, G. Reiner, C. Cremer, and E. H. K. Stelzer, "Aberrations in confocal fluorescence microscopy induced by mismatches in refractive index," *J. Microsc.* **169**, 391–405 (1993).
 16. C. J. R. Sheppard and P. Torok, "Effects of specimen refractive index on confocal imaging," *J. Microsc.* **18**, 366–374 (1997).
 17. M. Born and E. Wolf, *Principles of Optics* (Pergamon, Oxford, U.K., 1999).
 18. X. Gan and M. Gu, "Effective point-spread function for fast image modeling and processing in microscopic imaging through turbid media," *Opt. Lett.* **24**, 741–743 (1999).
 19. D. S. Wan, M. Rajadhyasksha, and R. H. Webb, "Analysis of spherical aberration of a water immersion objective: Application to specimens with refractive indices 1.33–1.40," *J. Microsc.* **197**, 274–284 (2000).
 20. I. J. Cox and C. J. R. Sheppard, "Digital image processing of confocal images," *Image Vision Comput.* **1**, 52–56 (1983).
 21. G. T. M. Van der Voort and K. C. Strasters, "Restoration of confocal images for quantitative image analysis," *J. Microsc.* **178**, 165–181 (1995).
 22. A. Diaspro, S. Annunziata, and M. Robello, "Single-pinhole confocal imaging of sub-resolution sparse objects using experimental point spread function and image restoration," *Microsc. Res. Tech.* **51**, 400–405 (2000).
 23. P. Torok and P. Varga, "Electromagnetic diffraction of light through a stratified medium," *Appl. Opt.* **36**, 2305–2312 (1997).
 24. A. Diaspro, S. Annunziata, M. Raimondo, P. Ramoino, and M. Robello "Single pinhole confocal laser scanning microscope operating as 3D image formation device in the study of biostructures," *IEEE Eng. Med. Biol. Mag.* **18**(14), 106–110 (1999).
 25. C. J. R. Sheppard, "Confocal imaging through weakly aberrating media," *Appl. Opt.* **39**, 6366–6368 (2000).